

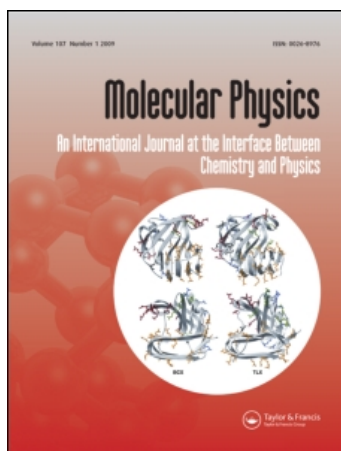
This article was downloaded by: [Jameson, Cynthia J.]

On: 7 July 2010

Access details: Access Details: [subscription number 924019383]

Publisher Taylor & Francis

Informa Ltd Registered in England and Wales Registered Number: 1072954 Registered office: Mortimer House, 37-41 Mortimer Street, London W1T 3JH, UK



Molecular Physics

Publication details, including instructions for authors and subscription information:

<http://www.informaworld.com/smpp/title~content=t713395160>

Diffusion of gases across lipid membranes with OmpA channel: a molecular dynamics study

Huajun Yuan^a; Cynthia J. Jameson^a; Sohail Murad^a

^a Department of Chemical Engineering, University of Illinois at Chicago, Chicago, IL 60607, USA

Online publication date: 07 July 2010

To cite this Article Yuan, Huajun , Jameson, Cynthia J. and Murad, Sohail(2010) 'Diffusion of gases across lipid membranes with OmpA channel: a molecular dynamics study', Molecular Physics, 108: 12, 1569 – 1581

To link to this Article: DOI: 10.1080/00268976.2010.484396

URL: <http://dx.doi.org/10.1080/00268976.2010.484396>

PLEASE SCROLL DOWN FOR ARTICLE

Full terms and conditions of use: <http://www.informaworld.com/terms-and-conditions-of-access.pdf>

This article may be used for research, teaching and private study purposes. Any substantial or systematic reproduction, re-distribution, re-selling, loan or sub-licensing, systematic supply or distribution in any form to anyone is expressly forbidden.

The publisher does not give any warranty express or implied or make any representation that the contents will be complete or accurate or up to date. The accuracy of any instructions, formulae and drug doses should be independently verified with primary sources. The publisher shall not be liable for any loss, actions, claims, proceedings, demand or costs or damages whatsoever or howsoever caused arising directly or indirectly in connection with or arising out of the use of this material.

RESEARCH ARTICLE

Diffusion of gases across lipid membranes with OmpA channel: a molecular dynamics study

Huajun Yuan, Cynthia J. Jameson and Sohail Murad*

Department of Chemical Engineering, University of Illinois at Chicago,
810 S. Clinton, Chicago, IL 60607, USA

(Received 9 February 2010; final version received 30 March 2010)

Molecular transport across biological membranes occurs in a range of important chemical and biological processes. The biological membrane can usually be modelled as a phospholipid bilayer, but to correctly represent biological transport, the embedded transmembrane proteins must also be included. In previous molecular simulation studies on transport of small gas molecules in dipalmitoylphosphatidylcholine (DPPC) bilayer membrane, a coarse-grained model was used to provide direct insight into collective phenomena in biological membranes. Coarse graining allowed investigation of longer time and length scales by reducing the degrees of freedom and employing suitable potentials. In this work, membranes that include transmembrane proteins are modelled. This allows one to compare the molecular transport across a lipid membrane with and without the assistance of transmembrane channels. Outer membrane protein A (OmpA) – a porin from *Escherichia coli* with a small pore size – was chosen in this study because its detailed structure is known, it has high stability and is known to form a nonspecific diffusion channel that permits the penetration of various solutes. In this work the pore characteristics and interaction between lipid and protein were investigated and transport of water and other small gas molecules within the channel were studied. The MD simulation results obtained are compared with previous simulation results and available experimental data. The results obtained from this study will lead to better understanding of protein functionality and advance the development of biochips and drug delivery systems.

Keywords: coarse grain; permeability; lipid membrane; OmpA

1. Introduction

Many biological processes involve molecular transport across biomembranes. Molecules can permeate these biomembranes using a variety of mechanisms, some of which are rather complex [1]. It is important to understand these transport mechanisms in biomembranes not only for their fundamental interest, but also for rational design of drug delivery systems, as well as for developing more efficient separation processes.

Lipid bilayers are one of the major structural elements of biological membranes which also play a key role as a protective barrier and substrate for other species, such as proteins. Lipid bilayers generally exhibit little permeability for hydrophilic solutes, including most nutrients. Therefore, biological membranes contain specific channel-forming proteins for the purpose of permitting the influx of nutrients and for the extrusion of waste products [2]. There is significant interest in investigating outer membrane proteins (OMPs), because they facilitate a variety of

functions including passive and active transport, signal transduction, catalysis, and targeted drug delivery [3].

Outer membrane protein A (OmpA) from *Escherichia coli* is a monomeric protein composed of two domains, including a transmembrane N-terminal domain of 171 residues forming an eight-stranded anti-parallel β -barrel [4]. OmpA is one of the most abundant outer membrane proteins in *Escherichia coli*, with about 10^5 copies in each cell [5]. There is considerable experimental data on the protein structure including its high resolution X-ray structure studied by Pautsch and Schulz [6,7]. OmpA is therefore an ideal protein for the study of dynamics of outer membrane proteins and membrane-protein interactions. Many experimental studies [8–11] and theoretical modelling studies [4,12–15] on the OmpA protein structure are available for comparison.

Experimental membrane permeation rates of small molecules can be measured by osmotic, NMR, and radio-tracer experiments, although the interpretation

*Corresponding author. Email: murad@uic.edu

of these results is often difficult [16]. Paula *et al.* [17] measured the permeability coefficient of potassium ions and small polar molecules as a function of membrane thickness. Jansen and Blume [18] compared diffusive and osmotic water permeation across phospholipids bilayers with different head groups and fatty acyl chains. Mathai *et al.* [19] studied structural determinants of water permeability through lipid membranes. Overall, the permeability across lipid membranes is affected by the properties of the small molecules, such as their molecular size, hydrophobicity and shape, and the properties of the lipid membranes.

Proteins embedded in lipid membranes account for about 25% of genes [20] and 50% of drug targets [21]. Despite their widespread presence, only around 100 high resolution structures of membrane proteins are known [13,22]. OmpA is a relatively simple bacterial outer membrane protein, and it was thought to primarily serve a structural role, as no continuous pore through the centre of the barrel could be observed in the crystal structure of OmpA [4]. However, several groups have reported ionic conductance [23–25], and many now believe that it may dynamically form ion-permeable pores across the membrane. Nikaido [2], for example, has categorized it as a slow porin since its permeability is slower than classical porins like OmpF. It is therefore important to further investigate the permeation through OmpA embedded in lipid membranes.

Molecular dynamics (MD) simulations are a powerful tool for producing details of permeation which are not available in experiments, such as structural and dynamic details. Marrink and Berendsen [26] used MD to calculate the permeability coefficients of water and a few small molecules across lipid membranes and proposed the inhomogeneous solubility–diffusion model. Recently, studies have been reported on investigations of the permeability of small uncharged molecules across lipid bilayers based on this model [27–30]. These investigators have used atomistic molecular dynamics simulation methods to study the local diffusion coefficients of different small gas molecules inside the lipid membrane and the effects of solute molecules and lipid molecules on the permeability. Although atomistic simulations now are able to reproduce and predict many fundamental properties of lipid membranes, the sizes of systems and timescales that can be investigated are still limited by current computers and algorithms. Coarse grain (CG) models in which we treat small groups of atoms as single particles, on the other hand, provide a promising approach to overcome some of these limitations in studying large biomolecular systems [31]. There are several coarse grain approaches available, which range

from qualitative, solvent-free models to models that include chemical specificity. Marrink and co-workers [32–34] recently developed a coarse-grained force field called MARTINI for simulation of lipids and surfactants. The MARTINI force field has been shown to reproduce semi-quantitatively fundamental structural and thermodynamic properties of lipid bilayers and proteins. Using this coarse-grained strategy, Bond and Sansom [12,14,35] have conducted studies on membrane proteins, such as the structure of membrane proteins, protein-membrane interactions, protein insertion and assembly.

The transport mechanism of small molecules across lipid bilayer membranes is still not well understood. Experimental results reported have not been in agreement with each other. Marrink and Berendsen [26,36] have proposed the inhomogeneous solubility–diffusion model which is an extension of the standard solubility–diffusion mechanism. Jansen and Blume [18] have proposed a mechanism which postulates that water transport mostly occurs across a transient pore of the bilayer. Thermal fluctuations lead to the spontaneous formation of transient pores across the membrane, which are nothing more than fluctuating defects in membranes. The occurrence of transient pores depends on the state of the membrane which is controlled by its intensive thermodynamic variables (e.g., temperature, pressure, electrostatic potential, and the chemical potential of the components). Under certain conditions, stable pore nucleation and growth could occur in bilayer membranes. However, we did not study such events here.

Recently, there have been several applications of CG simulations of membrane proteins, and results from these initial studies are very promising [3,14,37]. Although CG simulations may not be able to provide molecular details of these proteins and their pore gating mechanisms, they provide a very useful tool to study complex biomolecular phenomena at longer time and larger size scales. In previous studies on small molecule transport across lipid bilayer membranes without outer membrane proteins, we were successful in studying small molecule transport, with permeability results in satisfactory agreement with experimental values [38,39].

In a previous study, a coarse-grained model was used to investigate the gas permeation process through dipalmitoylphosphatidylcholine (DPPC) lipid bilayers [38]. In the present study the outer membrane protein A (OmpA) is included. The goal is to develop a fundamental understanding of how small molecules permeate such membranes and to gain insight about the various transport mechanisms. Here a molecular dynamics simulation is used with the coarse-grained

MARTINI force field for the lipid bilayer and OmpA to investigate the permeability of three small molecules, water, xenon, and oxygen, across the lipid bilayer with embedded OmpA. MD results are compared with previous MD studies of permeation without OmpA channels, and with available experimental results.

2. Method

2.1. Lipid and OMPA structures

We performed molecular dynamics simulations for a lipid bilayer system: DPPC (C₁₆), with OmpA [6] embedded. The details of the molecular structure are shown in Figure 1.

2.2. Models

The MARTINI CG force field is based on a four-to-one mapping, i.e. on average, four heavy atoms are represented by a single interaction site. We will only briefly summarize it here, since details are available in

the original papers of Marrink *et al.* [32–34] The model has four main types of interaction sites: polar (P), nonpolar (N), apolar (C), and charged (Q). Within a main type, subtypes are distinguished either by a letter denoting the hydrogen-bonding capabilities (d = donor, a = acceptor, da = both, o = non) or by a number indicating the degree of polarity (from 1 = lower polarity to 5 = higher polarity). For the lipid bilayers, we employ the Marrink *et al.* [33] mapping strategy; the phospholipid DPPC is modelled as 12 CG sites. For the OmpA, we employ the same mapping of amino acids to get coarse-grained proteins developed by Bond *et al.* [14] based on methods derived from Marrink *et al.* [32] The 1330 atomistic protein atoms in OmpA become 369 coarse-grained sites after mapping, as shown in Figure 2. The coarse-grained OmpA structure was obtained from the CG protein database developed by Sansom *et al.* [12].

All particle pairs i and j at distance r_{ij} interact via a Lennard–Jones (LJ) potential:

$$V_{LJ}(r_{ij}) = 4\epsilon_{ij} \left[\left(\frac{\sigma_{ij}}{r_{ij}} \right)^{12} - \left(\frac{\sigma_{ij}}{r_{ij}} \right)^6 \right]. \quad (1)$$

The well depth ϵ_{ij} depends on the interacting particle types and the value ranges from $\epsilon_{ij} = 5.6$ kJ/mol for interactions between strong polar groups to $\epsilon_{ij} = 2.0$ kJ/mol for interactions between polar and apolar groups mimicking the hydrophobic effect.

The effective size of particle is governed by the LJ parameter $\sigma = 0.47$ nm for all normal particle types except for the interaction between charged (Q type) and most apolar types (C1 and C2), where the range of repulsion is extended by setting $\sigma = 0.62$ nm. For protein side-chain ring-ring interactions, $\sigma = 4.3$ nm, and ϵ_{ij} is scaled to 75% of the standard value. In addition to LJ interactions, charged groups interact via a shifted coulombic potential function [40] with a relative dielectric constant $\epsilon_r = 15$ [33]:

$$U_{elec} = \frac{q_i q_j}{4\pi\epsilon_0\epsilon_r r}. \quad (2)$$

In the OmpA protein, some amino acids sites include charges [34]; for example, GLU and ASP carry a negative charge, ARG and LYS a positive charge; the overall OmpA is negatively charged ($-3e$). The effect of including counterions on the stability of the protein, while widely studied in atomistic simulations, is still not clearly understood. Drabik *et al.* [41] carried out tests and concluded that there was no clear evidence that counterions led to more stable protein secondary structures in simulations. In our studies, for simplicity, we therefore did not include counterions. The stability of the model was further confirmed by monitoring the drift in the RMSD results (see Section 2.4).

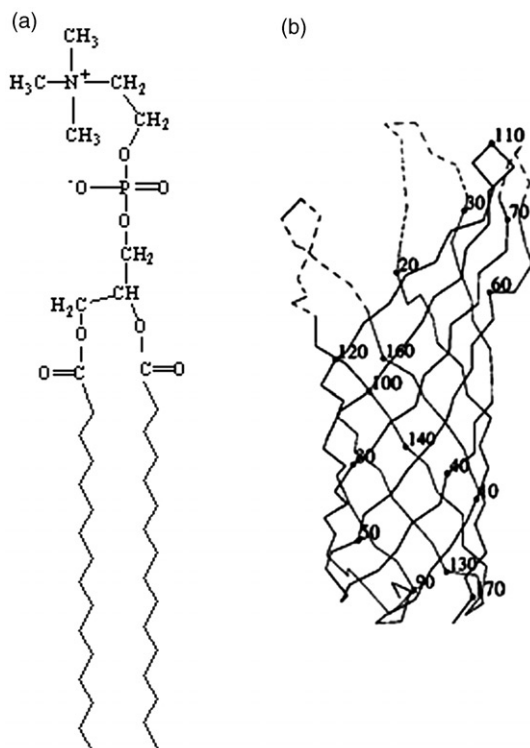


Figure 1. Molecular structures of (a) DPPC (C₁₆) lipid and (b) OmpA transmembrane domain: stereoview of the Calpha chain with every tenth residue labeled, highly mobile loop moieties are given as dashed lines [4].

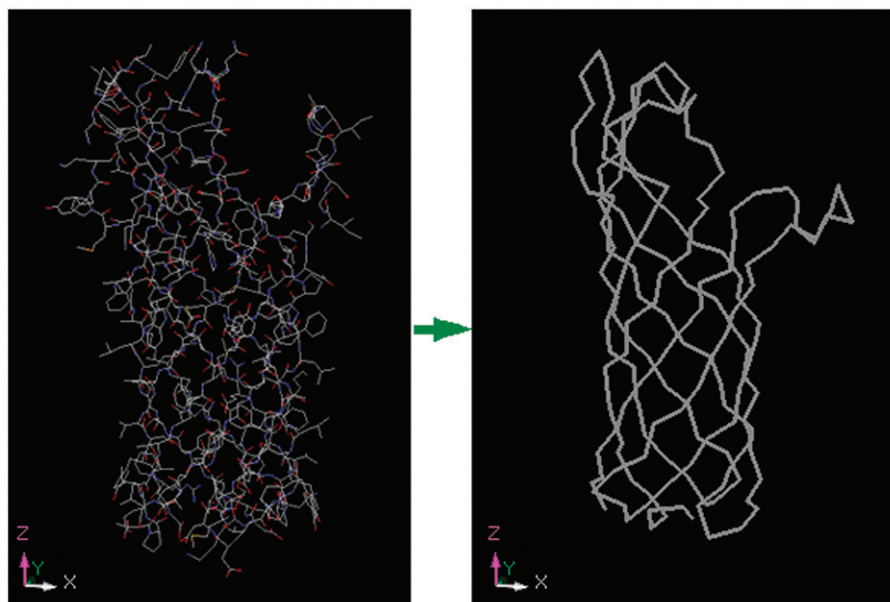


Figure 2. Coarse-grain mapping for OmpA. The atomistic OmpA coordinates were taken from pdb file 1BXW [4], the CG OmpA only shows the backbone.

In the simulations the non-bonded interactions are cut off at $r_{cut} = 1.2$ nm. The LJ potential is shifted from $r_{shift} = 0.9$ nm to 1.2 nm and the electrostatic potential is shifted from $r_{shift} = 0.0$ nm to 1.2 nm following a standard shift function [42]. Bonded interactions are described by the following set of potential energy functions acting between bonded site i, j, k , and l with equilibrium distance d_b , angle ϕ_a and dihedral angles ψ_d and ψ_{id} :

$$V_b = \frac{1}{2} K_b (d_{ij} - d_b)^2. \quad (3)$$

$$V_a = \frac{1}{2} K_a \{\cos(\varphi_{ijk}) - \cos(\varphi_a)\}^2. \quad (4)$$

$$V_d = K_d [1 + \cos(n\psi_{ijkl} - \psi_d)]. \quad (5)$$

$$V_{id} = K_{id} (\psi_{ijkl} - \psi_{id})^2. \quad (6)$$

Bonded interaction parameters in the MARTINI force field can be found in reference [34].

The small molecules we tested are water, xenon, oxygen and carbon dioxide. For water we use CG water parameters and for consistency, we also use similar central LJ models for oxygen and carbon dioxide. The potential parameters of the molecules studied are listed in Table 1.

For the cross-interactions between small molecule sites and CG sites including lipid/water and

Table 1. Potential parameters of gas molecules studied.

Molecule	Interaction Sites	σ (Å)	ϵ (k)	q (e)
Xe ^a	Central LJ	3.95	120	0
O ₂ ^b	Central LJ	3.36	228	0
CO ₂ ^c	Central LJ	3.72	236.1	0

Notes: ^aParameters from Ref. [43]

^bParameters from Ref. [44]

^cParameters from Ref. [45]

amino acids, we use the Lorentz-Berthelot mixing rules [46] as the initial starting point, and may modify the interaction parameters in the future if necessary to get a better description of the interactions. In the results presented here it was not found necessary.

2.3. Model validation

To validate the MARTINI force field used in this study, we carried out a comprehensive series of tests. A summary of the tests used in this study is given below. We monitored the self-assembly process of the lipid bilayer membrane with 128 DPPC molecules and 2000 water molecules, starting from random orientations and positions. This is a rather stringent test of the model. Snapshots of the configurations for 100 ns are shown in Figure 3, which clearly shows a lipid bilayer membrane forming spontaneously.

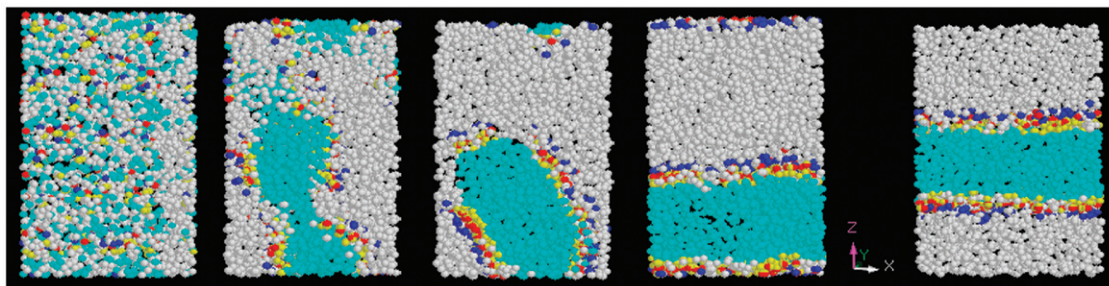


Figure 3. Simulated DPPC lipid membrane self-assembly process (blue dots represent the choline group, red the phospho group, yellow the glycol group, cyan the acyl chain group, while white dots are water molecules).

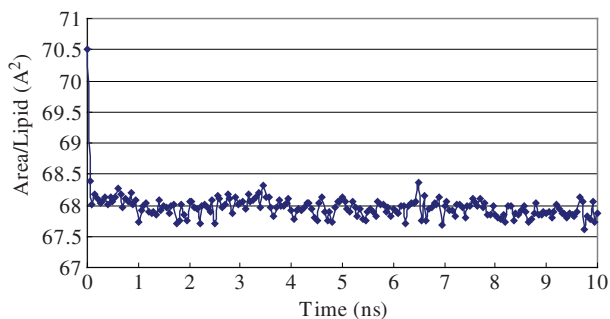


Figure 4. Simulation results for the area per lipid for the self-assembled DPPC lipid membrane at 323 K.

We then examined a range of properties of this membrane. Important quantities characterizing a lipid bilayer membrane are (a) the surface area per lipid; (b) the thickness of the membrane which may be characterized by providing the average distance between two extreme points such as phosphate groups on opposite sides of the bilayer; (c) the thickness of the interior, for example the projected distance along the bilayer normal for carbons on opposite sides of the bilayer. In a CG simulation, we can provide (a) and (b).

The area per lipid measured for the self-assembled DPPC at 323 K (50°C) was found to be 68 Å² (Figure 4), which agrees well with the experimental measurements which lie between 57 and 71 Å² [47].

The density profile of each component of the lipid was obtained during the simulation, which is shown in Figure 5, from which we obtained the distance between phosphate groups is 3.7 nm which is in close agreement with the experimental value of 3.85 nm [47].

If we assign electrons associated with each group, we can compare the electron density from the simulation with experimental values and other simulation results [47]. Although this comparison of probability profiles is not accurate due to the coarse graining, this permits a direct comparison with atomistic simulations. Our results in Figure 6 show qualitatively

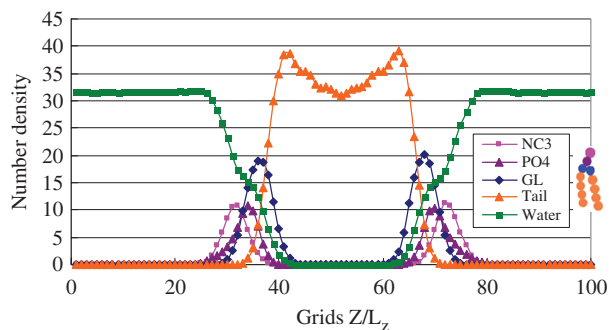


Figure 5. Simulation results for the density profile of components of self-assembled DPPC membrane along the Z direction.

consistent behaviour with the experimental electron density profile and also mimics reasonably well the atomistic profile.

Generally the conformation of the hydrocarbon tails of the lipid in a bilayer membrane is highly disordered. The conformational and orientational order/disorder can be quantified by various quantities in an atomistic simulation, including the very useful order parameter of C–H bond directions, but in a CG simulation only a limited number of indicators of internal order may be obtained from the simulation. One we have considered above is the probability distribution of different groups along the membrane normal axis, which gives some indication of the average alignment of the various parts of the lipid molecule. Another measure of the internal order of our lipid bilayer is the order parameter,

$$P_2 = \left\langle \frac{3 \cos^2 \theta - 1}{2} \right\rangle \quad (7)$$

where θ is the angle between the bond and normal to the bilayer. $P_2 = 1$ denotes perfect alignment, $P_2 = -0.5$ anti alignment, and $P_2 = 0$ a random orientation. Again, because we are using a coarse grained

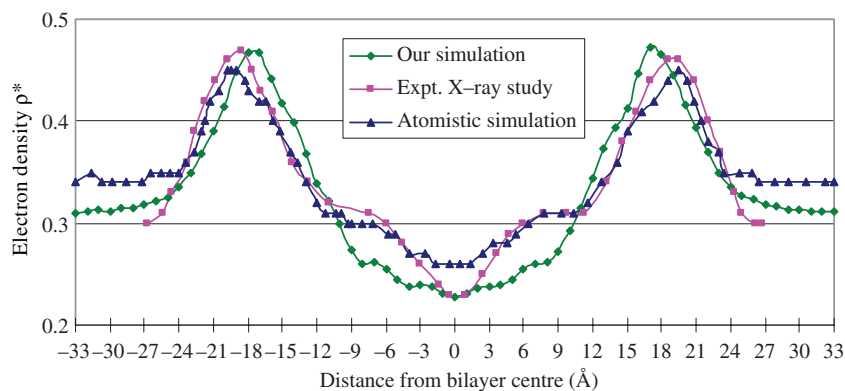


Figure 6. Comparison of simulated electron density (ρ^* in electrons/ \AA^3) with X-ray experimental measurements and atomistic simulation from reference [47].

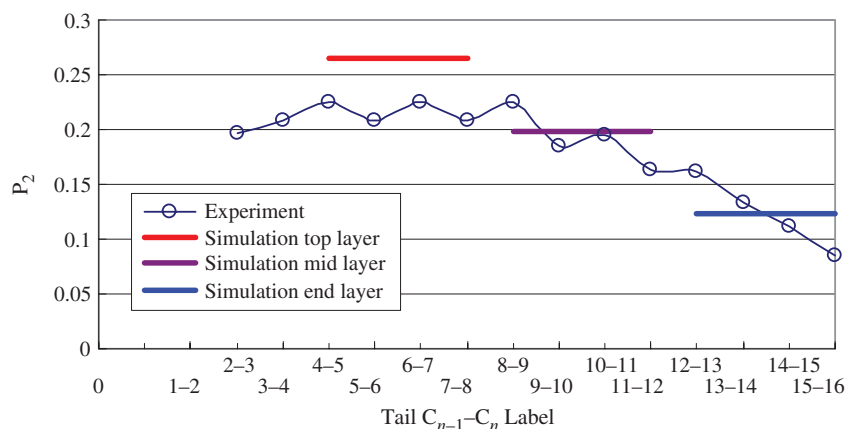


Figure 7. Comparison of calculated tail segment order parameter with experimental measurements [48].

scheme, the order parameter of our sites can not be compared directly with $C_{n-1} - C_n$ order parameters derived from experimental C-D order parameters [48]. The four sites that constitute the tail form three ‘bonds’ between them, and the order parameters for these can be effectively compared with experimental values. From the results shown in Figure 7, we can see that the coarse-grained model qualitatively reproduces the correct trends, with our lipid model being somewhat more highly aligned near the head than the actual DPPC lipid layer.

In summary, we feel a high level of confidence in the effectiveness of the coarse grained model used here.

2.4. Simulations of lipid bilayer with embedded OmpA

We performed molecular dynamic simulations of lipid bilayer DPPC systems with embedded OmpA. All the simulations were performed using the LAMMPS simulation package [49]. The dynamics in CG studies

are faster since CG interactions are much smoother compared with atomistic interactions. To ensure stability, we used a time step of 10 fs. The simulation system is shown in Figure 8 and consists of 205 lipid molecules and 4869 water molecules, with one OmpA N-terminal transmembrane protein represented by 369 CG sites. A typical simulation takes about 1.20 h per ns on an Intel Core2Quad CPU system. The OmpA-embedded DPPC bilayer is formed using a self-assembly method by Sansom *et al.* [14] and we fixed our simulation box size to be $8.55 \times 8.55 \times 12.5 \text{ nm}^3$. In our studies, the system was first equilibrated at 323 K, which allowed the transport of water molecules into the membrane. Subsequently gas molecules were added to the system to enable us to observe the transport of gas molecules. A Langevin thermostat (a frictional force is added to the conservative force to adjust the temperature) [50] was applied in the NVT ensemble to maintain the desired temperature. The density profiles of the DPPC, water and gas molecules were then measured as the system relaxed towards equilibrium. Additional validation tests (see also

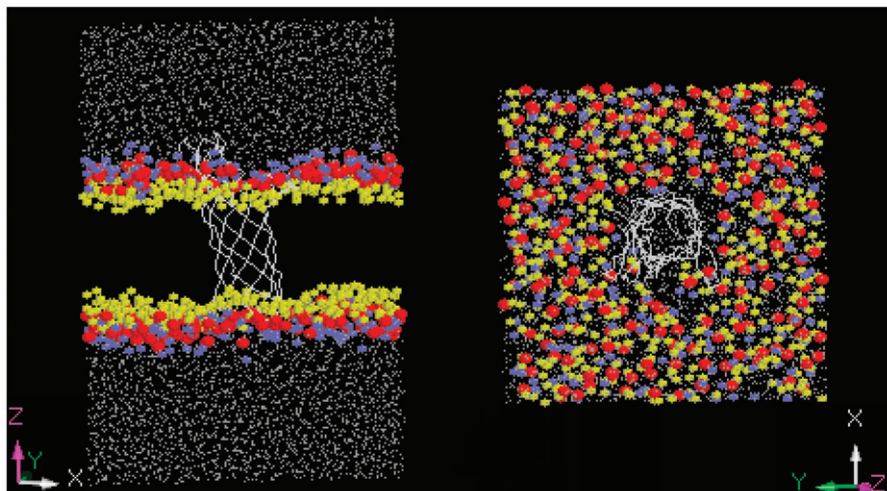


Figure 8. Side and top view of the simulation system for investigating permeability (OmpA is shown as the backbone. For DPPC, blue dots represent the choline group, red the phospho group, yellow the glycol group, white water while acyl chains are hidden for clarity).

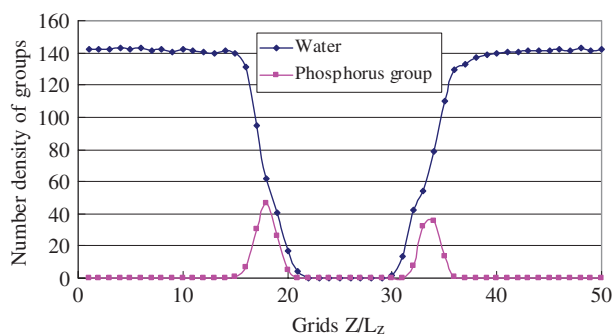


Figure 9. Lipid bilayer density test (along Z direction, blue points are number density of water, red points are number density of phosphorus head group).

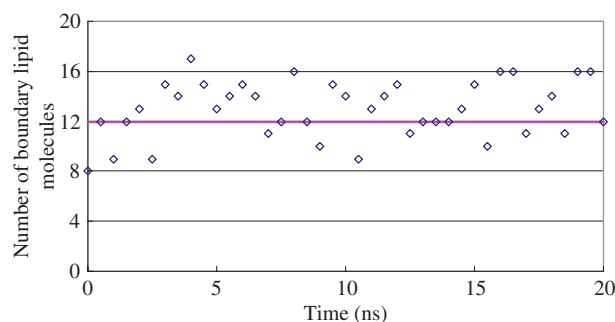


Figure 10. Results for the average number of lipid molecules in contact with OmpA in a 20 ns simulation.

Section 2.3) were then performed to ensure that the model correctly reproduced the experimental bulk properties, and agreed with other available atomistic simulation results and experimental measurements. These tests are summarized below.

We first examined the density of DPPC lipid bilayer, which can be obtained from the lipid thickness by measuring the distance between the two layers of phosphorus head groups. A typical density profile is shown in Figure 9.

From Figure 9, the measured distance between phosphate head groups is 4.0 nm, which is somewhat greater than the 3.7 nm we found in the absence of OmpA. The latter was in close agreement with the experimental value of 3.85 nm [47]. The embedded OmpA channel has an effect on the lipid bilayer thickness which is not unexpected.

Since the interaction between the lipid and embedded OmpA is important, we also calculated the average number of lipid molecules in contact with the protein surface. These are generally referred to as 'boundary' lipid molecules [49]. The result obtained is shown in Figure 10 for a simulation time of 20 ns with output frequency of 0.5 ns.

Our simulation showed that an average of 12 DPPC lipid molecules were in contact with the OmpA protein, which is consistent with the MD simulation result of 14 reported by Sansom *et al.* [51] for OmpA embedded in DMPC (dimyristoylphosphatidylcholine) bilayer. Our MD average of 12 DPPC lipid molecules in contact with OmpA protein is also in agreement with the experimental results for OmpA reconstituted in bilayers of spin-labelled dimyristoylphosphatidylglycerol, in which the stoichiometry of the motionally restricted lipids, 11 lipids/monomer for OmpA, is

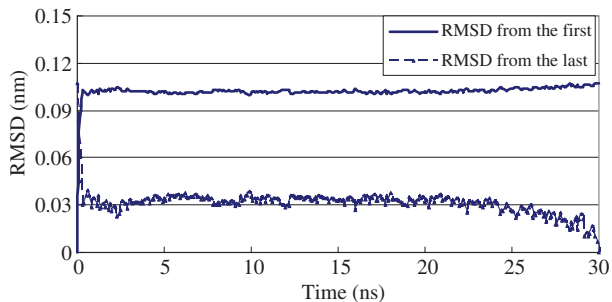


Figure 11. RMSD measurement of C-alpha backbone of OmpA for 30 ns simulation.

found to be constant irrespective of the total lipid/protein ratio in the sample [52].

We also measured the root mean square deviation (RMSD) of C-alpha atoms in the protein which is related to the stability of protein structure using the definition in [53]. This definition is somewhat different from the standard definition in that the smaller of the backward and forward values are used,

$$\text{RMSD} = \min_{T,R} \sqrt{\frac{\sum_i^{N_{\text{atoms}}} (r_i(t_0) - r_i(t))^2}{N_{\text{atoms}}}} \quad (8)$$

where N_{atoms} is the number of atoms whose positions are compared, $r_i(t)$ is the position of atom i at time t . By using the analysis of Stella and Melchionna [53], we cannot only calculate RMSD from $t_0=0$, but also calculate RMSD backward, i.e., compare with the final stable configuration. This enables us to have additional information about the relaxation and sampling mechanisms. We measured the RMSD of the backbone C-alpha atoms of OmpA after the system had equilibrated (stabilized) for 30 ns in the simulation. A typical result is shown in Figure 11 with an RMSD about 0.1 nm calculated forward and 0.03 nm calculated backward. From the time before RMSD reached a plateau, we find that the relaxation time for the system is about 200 ps.

Using the usual forward RMSD, Sansom *et al.* [12] measured the RMSD of C-alpha atoms in OmpA and obtained a value of 0.14 nm. Our measured RMSD is in reasonable agreement with their result (considering the error bars). Our results are also comparable with atomistic simulation results of RMSD reported by Khalid *et al.* [3] of about 0.2 nm. We also monitored the RMSD of the total configurational energy and obtained similar behaviour [53]. Overall, our simulation results agree reasonably well with both the available experimental values and other simulation results. This validation shows that both our model and our simulation scheme are qualitatively realistic, and

should provide realistic predictions of properties not previously measured.

3. Results and discussion

3.1. Open and closed OmpA pores

It is generally accepted that OmpA pores are dynamically formed. Bond and Sansom [4] have suggested the possibility of transient formation of a central pore by atomistic simulations. Hong *et al.* postulated the possibility of a functional channel-gating mechanism contributing to the survival of bacteria growing under osmotic stress [54].

In our studies we investigated the DPPC-OmpA-water system at 323 K, as described above. Our simulation system is shown in Figure 12. We modelled both open and closed pores in OmpA by changing the interaction parameters between water and OmpA. We have used the closed pore configuration to study membrane compressibility and stability; these results will be discussed in a future report [55]. Previous simulations have reported water configurations in nanochannels across lipid membranes. For example, Nielsen and Klein [31] observed water transport across a capped nanotube embedded in a lipid bilayer, and Khutorsky [56] simulated water across the Amphotericin B channel with a pore size of 8 Å which is very comparable with the OmpA with pore size about 10 Å [23]. Sansom *et al.* have simulated atomistic water structure and dynamics in channel-like cavities [57,58] using simplified channel models to study the microscopic properties of water in narrow pores, and the role of hydrophobicity/hydrophilicity in the entry of water into pores. Their simulation of OmpA indicated that a small conformational change may open it and allow water to permeate. Tieleman *et al.* [59] reported that the ratio of the diffusion coefficient in the pore to that in bulk solution varies as a function of pore radius. These simulations have provided details of water structures and dynamics in various channels, both artificial and protein. However, atomistic simulations are rather CPU intensive, therefore simulation times were usually only a few nanoseconds which allowed only one channel or sometimes only half of a channel to be simulated.

Although CG simulations may not be able to provide precise details for the open↔close pore mechanism, our goal is to mimic this process and test the effect of pore open/close status on transport rates so that we can later simulate larger systems with pores both open and closed. Experimental studies reported by Sugawara and Nikaido [23] show that only a small subset of OmpA molecules (2–3%) have an open channel.

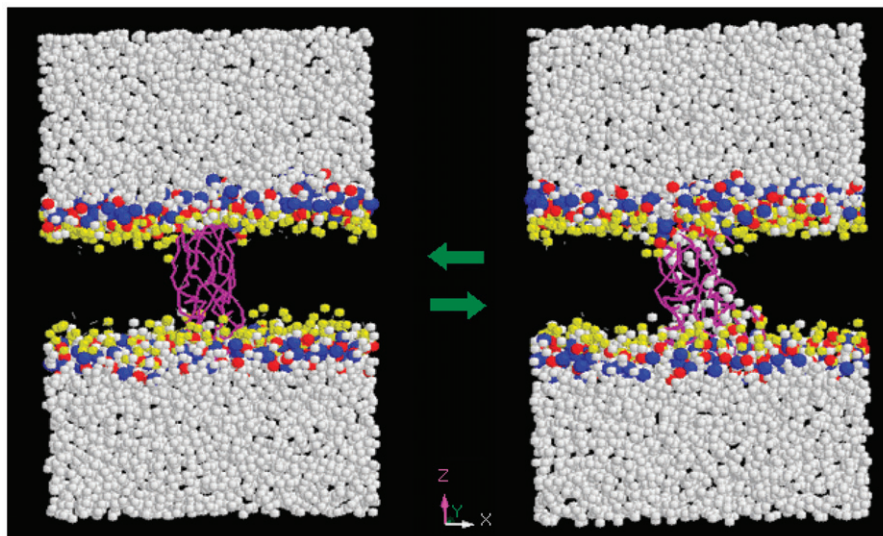


Figure 12. Water channel formed by OmpA. Closed (left), Open (right), blue dots represent the choline group, red the phosphate group, yellow the glycol group, white water molecules; acyl chains were hidden for clarity.

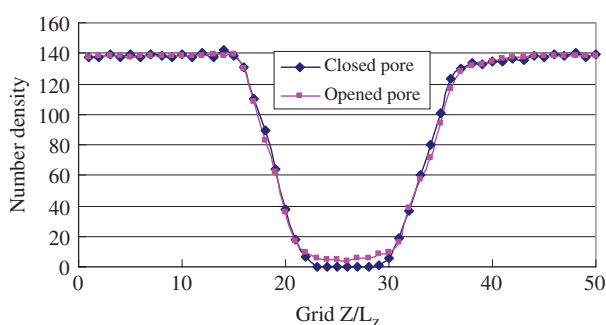


Figure 13. Simulation results for water density profile along the Z direction, Blue points represent a closed pore, while the red an opened pore.

To simulate these biological membranes more realistically, it may be necessary to have a fraction of OmpA pores in the open configuration, while the remaining OmpA can be in the closed configuration. Our present simulations employ the structure for open pore OmpA.

Since there is no further driving-force once the pore is filled with water, net transport (permeation) of water through the pore is not observed in our simulation system, but the density profile can provide us the information on how many water molecules are needed to fill the OmpA pore and the average density of water in the pores. A typical density profile is shown in Figure 13. The density profile of water is quite uniform in the middle of the pore, with an average density of water in OmpA channel of $0.027/\text{\AA}^3$. Khutorsky [56] *atomistically* simulated antibiotic amphotericin B channel with pore diameter of 8\AA in lipid membrane, a smaller

pore than our OmpA channel. Their simulated half-pore length was 25\AA which is shorter than the OmpA channel length of 57\AA . For computing efficiency, they neglected the hydrophobic exterior and the environment and only simulated those atoms that have actual contacts with water and ions. They reported an average water density in the channel of $0.020/\text{\AA}^3$ with some cross-sections of the channel containing three or four water molecules. Considering the different pore size and channel length, our coarse-grained simulation result is in good agreement with their atomistic results, and our somewhat higher numbers are attributable to the larger pore diameter of OmpA.

3.2. Gas permeation

The first small molecule we investigated was xenon. Xenon atoms in the ground state are spherical, with high polarizability that enhances dispersion forces. Because of its relatively simple atomic structure, xenon has been extensively used to study gas solubilities in organic liquids [60–62]. In our simulations, once the DPPC – OmpA – water system is equilibrated, 12 xenon atoms were introduced in the water compartment of the system. We chose a small number of gas molecules since the solubility of xenon in water is rather small at low pressures (up to 10 bar). Although solubility increases with pressure, high pressures on the bilayer can make the lipid bilayer membranes unstable. A snapshot of the system with gas molecules and OmpA-embedded lipid bilayer is shown in Figure 14.

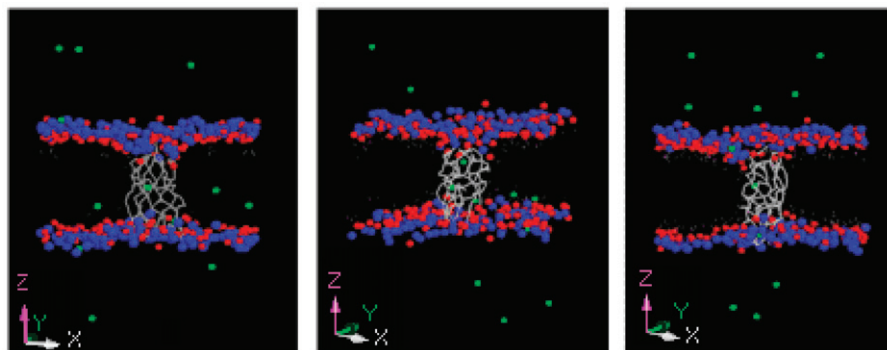


Figure 14. Snapshot of gas molecules in the simulation system (from left to right Xe, O₂, CO₂), green dots represent gas molecules, blue dots the choline group, red dots the phospho group, glycol group and acyl chain are hidden for clarity.

From Figure 14, we can observe clearly that the xenon is primarily permeating through the lipid bilayer with no xenon permeating through the OmpA channel. For oxygen and carbon dioxide, the preferred path appears to be through the OmpA channel. This is not surprising because of the molecular sizes of oxygen, carbon dioxide and xenon (see Table 1). For xenon, we did not observe any permeation through the channel because of its size. With a smaller particle size, it is easier for the oxygen or carbon dioxide to permeate through the protein channel.

The observed permeation percentages of gas molecules in OmpA–lipid system are shown in Table 2, where we find that Xe preferentially transports across the lipid bilayer itself, whereas CO₂ and O₂ transport through OmpA just as well. Although there are no experimental results to compare with these predictions, our previous validation of the model leads us to believe these are reliable predictions.

The density histogram of gas molecules along the z direction (normal to lipid bilayer surface) is shown in Figure 15. From the histogram, it can be seen that Xe was blocked in the entrance of the channel, but O₂ and CO₂ were able to permeate through the channel.

We next compared the permeation rate of these gases in lipid membranes with and without the OmpA protein channel. The permeation rate of gas molecules through biomembranes is relatively small. To observe the permeation of gas molecules across the membrane quantitatively would either require large concentration of gas molecules (which is not realistic except under very high pressures which may affect the stability of the biomembrane) or very large systems, or long simulation times. We studied low-pressure (below 10 bar) solutions but carried out simulations for 100 ns. Our simulations gave us a relatively reliable qualitative picture of the permeation rates in these systems. Marrink *et al.* [26] also mentioned the difficulty of

Table 2. Observed permeation events of gas molecules in OmpA–lipid systems.

Gas	Permeation through OmpA (%)	Permeation through DPPC lipid bilayer (%)
Xe	0.0	100.0
CO ₂	53.8	46.2
O ₂	62.5	37.5

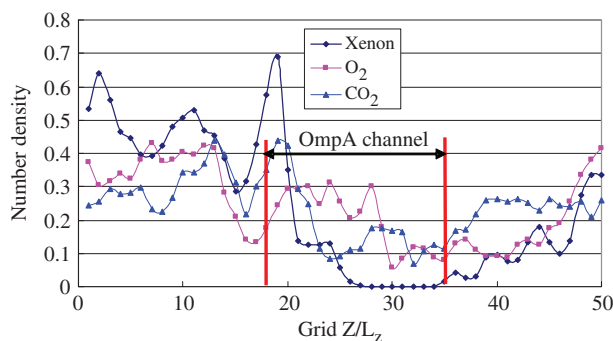


Figure 15. Comparison of density profiles of Xe, O₂ and CO₂ molecules along the direction normal to the lipid bilayer surface.

making quantitative comparison when permeation occurs at a low rate.

With OmpA, gas molecules have two permeation pathways, either through the OmpA pore, or through the lipid bilayer directly. Over a 100 ns simulation, we monitored the permeation of various gases in both types of membranes and compared with gas permeation through pure lipid bilayer from our previous simulations [38], and the results are summarized in Table 3.

From our results we can observe that in the DPPC membranes as well as the OmpA channel, the

Table 3. Observed permeation events of gas molecules across lipid bilayer and lipid/OmpA system.

Gas	Permeation through lipid/OmpA system (DPPC,OmpA)	Permeation through only DPPC lipid bilayer
Xenon	4 (4,0)	4
CO ₂	13 (6,7)	10
O ₂	24 (9,15)	21

permeation rate increases as the molecular size decreases, as expected. However, the rate of increase is much more dramatic in the OmpA channel (0 → 15) than the DPPC bilayer (4 → 9) which offers a much more tortuous path to the molecules. Overall it does not appear that the permeability of small molecules is particularly enhanced by the presence of the OmpA channel, although there is a consistent increase of about 20% in our system with stoichiometry of 1 OmpA/205 lipid (approximately 4 percent of the surface is occupied by the OmpA channel).

3.3. Calculations of gas permeability through lipid with and without OmpA

To enable comparisons with experimental measurements, we used a definition of gas permeability developed by us previously [38], and also used by others [63]. This definition is especially useful in coarse grained studies, since it eliminates the need for time scaling, which otherwise is necessary in coarse grained studies.

$$P = \frac{D_{\perp}}{D_{//}} \quad (9)$$

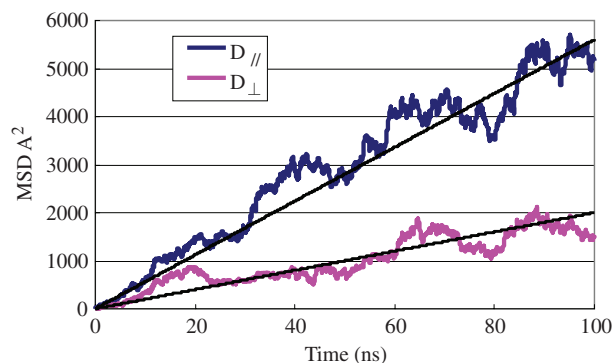
$$\text{Here } D_{\perp} = D_z = \frac{1}{2 \times 1} \lim_{t \rightarrow \infty} \frac{\langle |r(t) - r(0)|^2 \rangle_z}{t} \quad (10)$$

and

$$D_{//} = D_{x+y} = \frac{1}{2 \times 2} \lim_{t \rightarrow \infty} \frac{\langle |r(t) - r(0)|^2 \rangle_{x+y}}{t} \quad (11)$$

D_{\perp} is the diffusion coefficient in the direction perpendicular into the bilayer surface, which represents the ability of gas molecules to move along the Z axis in our simulation box, whereas $D_{//}$ is the diffusion coefficient in the direction parallel to the bilayer surface on the XY plane.

If the membrane is impermeable, the gas molecules can only move on the XY plane, the ratio of $\frac{D_{\perp}}{D_{//}}$ will be zero. On the other hand, if there is no resistance and the gas molecules can permeate freely through the

Figure 16. MSD for diffusion coefficient calculations of O₂ for 100 ns simulation.

membrane, the ratio will be 1. Usually the permeability will be between 0 and 1.

We can compare the permeability obtained from our simulation results directly with experimental results without additional concerns about the conversion of the coarse-grain time scales to real time, a well known problem in CG simulations [33]. By using such a definition, the use of periodic boundary conditions does not interfere with permeability calculation since the permeability obtained is only affected by the inhomogeneous lipid-water interface.

Using Equation (9), we can calculate the permeability via the mean square displacement (MSD) curve generated during the simulation. A typical MSD curve of oxygen is shown in Figure 16, which shows the MSD curves parallel ($D_{//}$) and perpendicular to the membrane surface (D_{\perp}).

The calculated permeability of different gases so obtained is listed in Table 4 and also compared with permeability results without the OmpA protein channel.

From Table 4, we can see the effect of the OmpA channel on gas permeability. Although we did not observe xenon atoms transported across the OmpA channel, they can still permeate through the water-lipid interface. We observed the xenon permeability increased in the OmpA/lipid system. This is probably attributable to the change in lipid structure near the protein lipid interface, since all xenon atoms permeate through the lipid membrane via dynamically formed pores at the water-lipid surface. The frequency of dynamically formed pores is affected by the protein embedded in the membrane. For CO₂ a similar effect (an increase) is observed primarily because of the availability of the OmpA channel. For oxygen, the effect is relatively small. Because of its smaller size it can readily permeate both the channel and the membrane. Based on the results of our simulations, the overall physics of membrane permeation by gases is

Table 4. Permeability of gas molecules in lipid and OmpA–lipid systems.

Gas	Permeability through DPPC	Permeability through DPPC with OmpA
Xe	0.334 ± 0.06	0.548 ± 0.04
CO ₂	0.464 ± 0.07	0.65 ± 0.10
O ₂	0.775 ± 0.11	0.714 ± 0.09

straightforward and easily understood as a consequence of lateral area fluctuations. In some cases (not Xe) additional permeation occurs through pores of transmembrane proteins embedded in the membrane. These proteins also affect permeation through the lipid bilayer via protein–lipid interactions which change lipid structure near the proteins. Our studies do not include active transport, where the mechanism of permeation can be much more complicated.

We further validate our simulations by comparison with experiments. Subczynski *et al.* [39] have reported an experiment to measure permeability of oxygen through a Chinese hamster ovary (CHO) plasma membrane using spin-labelled stearic acid incorporated into the membrane at very low concentrations. They calculated permeability as the ratio of the permeability coefficient across the membrane to the permeability across the water layer, which is comparable with our calculation of permeability (Equation (9)).

The comparison of our calculated results with their experimental results is shown in Figure 17. We find that our result at 323 K is consistent with their experimental results at three lower temperatures. The results confirm our previous observations (discussed above) about the insensitivity of the oxygen permeability to the presence of OmpA channels.

4. Conclusions

We have investigated gas permeation in OmpA-embedded DPPC lipid bilayer systems by using coarse-grained molecular dynamics simulations. Our results are in satisfactory agreement with available experimental data, and with previous simulations. We have also reported results that have not previously been measured.

This study has shown that the MARTINI force field can be successfully used to simulate small molecule permeation in OmpA-embedded biomembranes and provides generally reliable results. We observed that the relative permeability is directly related to the size and competitive energy barriers of OmpA and lipid bilayers.

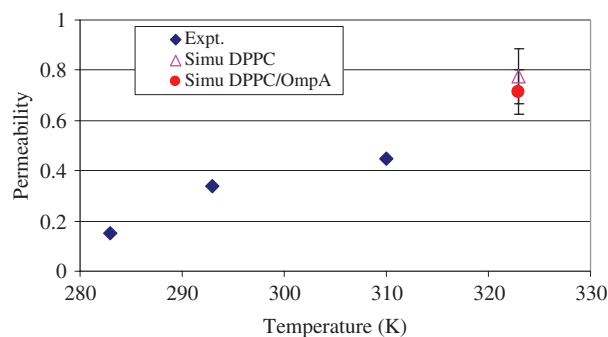


Figure 17. Comparison of permeability of O₂ through DPPC bilayer and DPPC/OmpA bilayer, blue diamonds represent experiments from [39]; pink triangle simulation result for pure DPPC bilayer; red circle simulation result for DPPC bilayer with embedded OmpA channel.

Our results also point to the need for additional experimental results to further refine/develop models for such systems.

Note

All figures can be viewed in colour online.

Acknowledgements

We thank the reviewer for many helpful and substantial comments and suggestions. This research has been funded by a grant from the Office of Basic Energy Science, Department of Energy [Grant No. DE-FG02-08ER46538].

References

- [1] E.A. Disalvo and S.A. Simon, *Permeability and Stability of Lipid Bilayers* (CRC Press, Boca Raton, Florida, 1995).
- [2] H. Nikaïdo, *Microbiol. Mol. Biol. R.* **67**, 593 (2003).
- [3] S. Khalid, P.J. Bond, T. Carpenter and M.S.P. Sansom, *BBA - Biomembranes* **1778**, 1871 (2008).
- [4] P.J. Bond, J.D. Faraldo-Gomez and M.S.P. Sansom, *Biophys. J.* **83**, 763 (2002).
- [5] P.J. Bond and M.S.P. Sansom, *J. Mol. Biol.* **329**, 1035 (2003).
- [6] A. Pautsch and G.E. Schulz, *Nat. Struct. Biol.* **5**, 1013 (1998).
- [7] A. Pautsch and G.E. Schulz, *J. Mol. Biol.* **298**, 273 (2000).
- [8] W.A. Woodruff and R.E. Hancock, *J. Bacteriol.* **171**, 3304 (1989).
- [9] M.S.P. Sansom, K.A. Scott and P.J. Bond, *Biochem. Soc. Trans.* **36**, 27 (2008).
- [10] A.H. Delcour, *FEMS. Microbiol. Lett.* **151**, 115 (1997).
- [11] A. Arora, F. Abildgaard, J.H. Bushweller and L.K. Tamm, *Nat. Struct. Mol. Biol.* **8**, 334 (2001).

- [12] M.S.P. Sansom, K.A. Scott and P.J. Bond, *Biochem. Soc. T.* **36**, 27 (2008).
- [13] P.J. Bond, J. Holyoake, A. Ivetac, S. Khalid and M.S.P. Sansom, *J. Struct. Biol.* **157**, 593 (2007).
- [14] P.J. Bond and M.S.P. Sansom, *J. Am. Chem. Soc.* **128**, 2697 (2006).
- [15] T. Lazaridis, *J. Chem. Theory. Comput.* **1**, 716 (2005).
- [16] A. Finkelstein (ed.) *Water Movement Through Membrane Channels*, Vol. 21 (Academic Press, New York, 1984).
- [17] S. Paula, A.G. Volkov, A.N. Van Hoek, T.H. Haines and D.W. Deamer, *Biophys. J.* **70**, 339 (1996).
- [18] M. Jansen and A. Blume, *Biophys. J.* **68**, 997 (1995).
- [19] J.C. Mathai, S. Tristram-Nagle, J.F. Nagle and M.L. Zeidel, *J. Gen. Physiol.* **131**, 69 (2007).
- [20] E. Wallin and G. Von Heijne, *Protein. Sci.* **7**, 1029 (1998).
- [21] G.C. Terstappen and A. Reggiani, *Trends. Pharmacol. Sci.* **22**, 23 (2001).
- [22] S.H. White, *Protein Sci* **13**, 1948 (2004).
- [23] E. Sugawara and H. Nikaido, *J. Biol. Chem.* **267**, 2507 (1992).
- [24] E. Sugawara and H. Nikaido, *J. Biol. Chem.* **269**, 17981 (1994).
- [25] E. De Saint, S. Julien, N. Orange and G. Molle, *BBA - Biomembranes* **1145**, 119 (1993).
- [26] S.J. Marrink and H.J.C. Berendsen, *J. Phys. Chem.* **100**, 16729 (1996).
- [27] W. Shinoda, M. Mikami, T. Baba and M. Hato, *J. Phys. Chem. B* **108**, 9346 (2004).
- [28] D. Bemporad, C. Luttmann and J.W. Essex, *Biophys. J.* **87**, 1 (2004).
- [29] T. Sugii, S. Takagi and Y. Matsumoto, *J. Chem. Phys.* **123**, 184714 (2005).
- [30] Y. Wang, J. Cohen, W.F. Boron, K. Schulten and E. Tajkhorshid, *J. Struct. Biol.* **157**, 534 (2007).
- [31] S.O. Nielsen, C.F. Lopez, G. Srinivas and M.L. Klein, *J. Phys.: Condensed Matter* **16**, R481 (2004).
- [32] S.J. Marrink, A.H. de Vries and A.E. Mark, *J. Phys. Chem. B* **108**, 750 (2004).
- [33] S.J. Marrink, H.J. Risselada, S. Yefimov, D.P. Tieleman and A.H. de Vries, *J. Phys. Chem. B* **111**, 7812 (2007).
- [34] L. Monticelli, S.K. Kandasamy, X. Periole, R.G. Larson, D.P. Tieleman and S.-J. Marrink, *J. Chem Theory Comput.* **4**, 819 (2008).
- [35] P. Bond, J. Holyoake, A. Ivetac, S. Khalid and M. Sansom, *J. Struct. Biol.* **157**, 593 (2007).
- [36] S.J. Marrink and H.J.C. Berendsen, *J. Phys. Chem.* **98**, 4155 (1994).
- [37] A.Y. Shih, A. Arkhipov, P.L. Freddolino and K. Schulten, *J. Phys. Chem. B* **110**, 3674 (2006).
- [38] H. Yuan, C.J. Jameson and S. Murad, *Mol. Simulat.* **35**, 953 (2009).
- [39] W.K. Subczynski, L.E. Hopwood and J.S. Hyde, *J. Gen. Phys.* **100**, 69 (1992).
- [40] E. Lindahl, B. Hess and D. van der Spoel, *J. Mol. Model.* **7**, 306 (2001).
- [41] P. Drabik, A. Liwo, C. Czaplewski and J. Ciarkowski, *Protein Eng. Des. Sel.* **14**, 747 (2001).
- [42] R. Baron, A.H. Devries, P.H. Hunenberger and W.F. Vangunsteren, *J. Phys. Chem. B* **110**, 15602 (2006).
- [43] M. Bohn, S. Lago, J. Fischer and F. Kohler, *Fluid Phase Equilibr.* **23**, 137 (1985).
- [44] M. Krishnamurthy, S. Murad and J.D. Olson, *Mol. Simulat.* **32**, 11 (2006).
- [45] H. Higashi, Y. Iwai and Y. Arai, *Fluid Phase Equilibr.* **234**, 51 (2005).
- [46] G.C. Maitland, M. Rigby and E.B. Smith, *Intermolecular Forces: Their Origin and Determination* (Clarendon Press, Oxford, 1981).
- [47] J.F. Nagle and S. Tristram-Nagle, *Biochim. Biophys. Acta* **1469**, 159 (2000).
- [48] J.P. Douliez, A. Leonard and E.J. Dufourc, *Biophys. J.* **68**, 1727 (1995).
- [49] S. Plimpton, *J. Comput. Phys.* **117**, 1 (1995).
- [50] T. Schneider and E. Stoll, *Phys. Rev. B* **17**, 1302 (1978).
- [51] M.S.P. Sansom, P.J. Bond, S.S. Deol, A. Grottesi, S. Haider and Z.A. Sands, *Biochem. Soc. T.* **33**, 916 (2005).
- [52] M. Ramakrishnan, C.L. Poczanski, J.H. Kleinschmidt and D. Marsh, *Biochemistry* **43**, 11630 (2004).
- [53] L. Stella and S. Melchionna, *J. Chem. Phys.* **109**, 3 (1998).
- [54] H. Hong, G. Szabo and L.K. Tamm, *Nat Chem Biol* **2**, 627 (2006).
- [55] H. Yuan, C.J. Jameson, S. Murad, in preparation (2010).
- [56] V. Khutorsky, *Biophys. J.* **71**, 2984 (1996).
- [57] M.S.P. Sansom, I.D. Kerr, J. Breed and R. Sankaramakrishnan, *Biophys. J.* **70**, 9 (1996).
- [58] M.S.P. Sansom, P. Bond, O. Beckstein, P.C. Biggin, J. Faraldo-Gomez, R.J. Law, G. Patargias and D.P. Tieleman, *Novartis Found. Sympos.* **245**, 66 (2002).
- [59] D.P. Tieleman, P.C. Biggin, G.R. Smith and M.S.P. Sansom, *Quart. Rev. Biophys* **34**, 88 (2001).
- [60] H. Yuan, S. Murad, C.J. Jameson and J.D. Olson, *J. Phys. Chem. C* **111**, 15771 (2007).
- [61] H. Yuan, C.J. Jameson, S.K. Gupta, J.D. Olson and S. Murad, *Fluid Phase Equilibr.* **269**, 73 (2008).
- [62] G.L. Pollack, R.P. Kennan, J.F. Himm and P.W. Carr, *J. Chem. Phys.* **90**, 6569 (1989).
- [63] A. Khakimov, M.A. Rudakova, M.M. Dorodigitskii and A.V. Filippov, *Biophys. J.* **53**, 147 (2008).